



# One Electron Multiple Proton Transfer in Model Organic Donor–Acceptor Systems: Implications for High-Frequency EPR

Kristy L. Mardis, et al. [full author details at the end of the article]

Received: 26 June 2020 / Revised: 3 August 2020 / Published online: 1 October 2020

© This is a U.S. government work and not under copyright protection in the U.S.; foreign copyright protection may apply 2020

## Abstract

EPR spectroscopy is an important spectroscopic method for identification and characterization of radical species involved in many biological reactions. The tyrosyl radical is one of the most studied amino acid radical intermediates in biology. Often in conjunction with histidine residues, it is involved in many fundamental biological electron and proton transfer processes, such as in the water oxidation in photosystem II. As biological processes are typically extremely complicated and hard to control, molecular bio-mimetic model complexes are often used to clarify the mechanisms of the biological reactions. Here, we present theoretical calculations to investigate the sensitivity of magnetic resonance parameters to proton-coupled electron transfer events, as well as conformational substates of the molecular constructs which mimic the tyrosine–histidine (Tyr–His) pairs found in a large variety of proteins. Upon oxidation of the phenol, the Tyr analog, these complexes can perform not only one-electron one-proton transfer (EPT), but also one-electron two-proton transfers (E2PT). It is shown that in aprotic environment the  $g_X$ -components of the electronic  $g$ -tensor are extremely sensitive to the first proton transfer from the phenoxyl oxygen to the imidazole nitrogen (EPT product), leading to a significant increase of the  $g_X$ -value of up to 0.003, but are not sensitive to the second proton transfer (E2PT). In the latter case, the change of the  $g_X$ -value is much smaller (ca. 0.0001), which is too small to be distinguished even by high-frequency EPR. The  $^{14}\text{N}$  hyperfine values are also too similar to allow differentiation between the different protonation states in EPT and E2PT. The magnetic resonance parameters were also calculated as a function of the rotation angles around single bonds. It was demonstrated that rotation of the phenoxyl group results in large positive changes ( $>0.001$ ) in the  $g_X$ -values. Analysis of the data reveals that the main source of these changes is related to the strength of the H-bond between phenoxyl oxygen and the proton(s) on  $\text{N}_1$  and  $\text{N}_2$  positions of the imidazole.

**Electronic supplementary material** The online version of this article (<https://doi.org/10.1007/s00723-020-01252-8>) contains supplementary material, which is available to authorized users.

## 1 Introduction

In the last decades, EPR spectroscopy experienced extensive development of its instrumentation and methodology as well as a rapid growth in applications [1–11]. Part of these efforts was focused on the increase of information which can be extracted from the EPR spectra. In contrast to modern NMR spectroscopy, EPR cannot currently be considered a truly analytical technique in the sense that in most cases spectra alone do not allow quick conclusions about molecular structures or easy quantification of several species in a mixture. This predominantly relates to the low specificity of the EPR spectra, i.e., only in a few cases can EPR spectral data be directly related to the structure of the paramagnetic center under study. The analysis of EPR data is usually carried out by time-intensive interactive computer simulation of the experimental spectra. In the simplest cases, like small organic radicals in liquid solutions, where all anisotropic interactions are averaged out due to fast tumbling, the data extraction can often be done quite accurately, and the molecular structure may be directly identified [12]. However, once the molecule becomes larger and possesses more magnetic nuclei, more sophisticated multiple resonance methods like electron nuclear double resonance (ENDOR) are required to determine the structure [12–15]. In cases of frozen solution, where typically many anisotropic interactions are present, the analysis becomes considerably more complex. If molecules containing atoms with large spin–orbit coupling (like transition metals) are involved, or several unpaired electrons are present, data analysis quickly becomes very challenging as for any ill-defined problem with a large parameter space. To simplify this problem and make the analysis reliable, some of the parameters must be determined from independent experiments using different and often more advanced techniques.

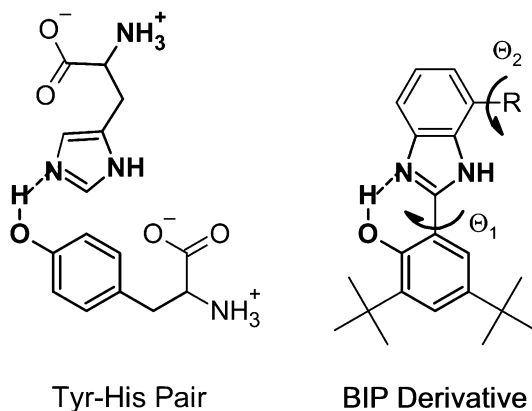
A number of these advanced approaches, which effectively increase spectral resolution of the EPR technique, were recently developed. Among them are: high-frequency (HF) EPR to resolve  $g$ -tensor components and separate overlapping spectra from different species; multi-frequency EPR to increase reliability of the extracted EPR parameters; time-resolved and pulsed technique to characterize transient species and relaxation properties of the paramagnetic species; pulsed ENDOR, ESEEM and HYSCORE to gain information on hyperfine interaction not resolved in the EPR spectra; pulsed ELDOR to determine distance and mutual orientation of spin centers [2–7, 11, 16–20]. Prof. Lebedev and his co-workers were among the first to realize the power of HF EPR for applications in chemistry and biology, and pioneered the instrumental and methodological development of HF EPR [21–25].

While extraction of spectroscopic parameters from EPR spectra has become more reliable, there is still a fundamental problem in determining the geometric and electronic structure of the paramagnetic center based on the parameters of the spin Hamiltonian used in EPR spectroscopy [2, 6, 7, 26]. Therefore, computational approaches are essential to provide the spin Hamiltonian parameters for particular molecular and electronic structures [27–29]. Depending on the accuracy required and the complexity of the system, different levels of theory can be

used. For systems of interest in the fields of catalysis and biological active sites, simple and computationally efficient semi-empirical analysis would be attractive except it often fails for the open shell transition metals in many of those systems. On the other end, high level ab initio wave function-based methods cannot be applied in most cases for biology and catalysis due to the enormous computational demands for treating large systems. Thus, using density functional theory (DFT) for the calculation of the molecular structure (geometry), electronic structure, and magnetic resonance parameters of EPR-active centers is often an excellent compromise of accuracy and computational demands [28, 30–32]. The validation and identification of the “real” geometric and electronic structure of paramagnetic centers in this case has to be done by careful comparison of the experimental and theoretically calculated parameters.

One prominent example where the combination of (HF) EPR and DFT calculations can be applied is the identification of the mechanism of light-induced proton-coupled electron transfer (PCET) process in the tyrosine–histidine (Tyr–His) pair (Scheme 1) in photosystem II (PS II) [33–38]. PS II is a very large transmembrane protein responsible for water oxidation and oxygen production [39–41]. A Tyr–His pair serves as a charge mediator for electron transfer from the oxygen-evolving Mn-containing complex to the oxidized primary donor, which is a chlorophyll dimer. Upon oxidation, Tyr donates a proton to its H-bonded His partner, thus forming a tyrosyl radical. HF EPR studies at low temperature clearly point to the complexity of this PCET process in PSII [38, 42, 43]. The low temperature mechanism of PCET on the molecular level was understood based on the combination of HF EPR experiments and extensive theoretical modeling of EPR parameters for the Tyr–His mimic, designed by the ASU group (Scheme 1) [44, 45]. The displacement of the proton from the Tyr oxygen to the nearest nitrogen of a His takes place upon light-induced Tyr oxidation [45]. At very low temperatures, below 10 K, this is a stable configuration. But upon annealing, the nearest environment of the tyrosyl radical relaxes and rearranges the H-bond to the tyrosyl oxygen. As a consequence, the  $g_x$  component of the  $g$ -tensor increases by about 0.001, which was confirmed by computational modeling [45, 46].

**Scheme 1.** Structures of a neutral tyrosine–histidine (Tyr–His) pair and a benzimidazole–phenol (BIP) derivative mimicking the Tyr–His pair. Upon electron transfer of the tyrosine or phenol to the neighboring imidazole ring, proton transfer and changes in H-bonding take place. The dihedral angles  $\Theta_1$  and  $\Theta_2$  are defined as shown for the BIP derivative



Besides its importance for PSII, tyrosyl radicals are the most frequently reported free radical in proteins [36, 47–51]. They are involved in many important enzymatic reactions in biology. While the dependence of the tyrosyl radical  $g$ -tensor on the strength and number of the H-bonds to oxygen is well studied in many biological systems and their synthetic analogs, there are still several important unanswered questions. In particular, in aprotic environments where external protons are not available to form hydrogen bonds with the oxygen or nitrogen atoms in the tyrosyl radicals or Tyr–His pairs, the extent of the influence of hydrogen bonding to remote nitrogen or conformation changes in the second and third coordination spheres on the magnetic resonance parameters is unknown. Recently, the ASU group developed more complex PCET model systems based on Tyr–His couples which can demonstrate not only one-electron one-proton transfer (EPT), but also one-electron two-proton (E2PT) and one-electron three-proton (E3PT) transfer, upon oxidation of the phenol, which operates as the Tyr analog [44, 52–55]. Thus, for the Tyr–His mimics shown in Fig. 1, the first proton transfer from phenoxyl oxygen to imidazole nitrogen  $N_1$  takes place upon oxidation (EPT product). The second proton transfer occurs from imidazole nitrogen  $N_2$  to  $N_3$  (E2PT product). While the first proton transfer

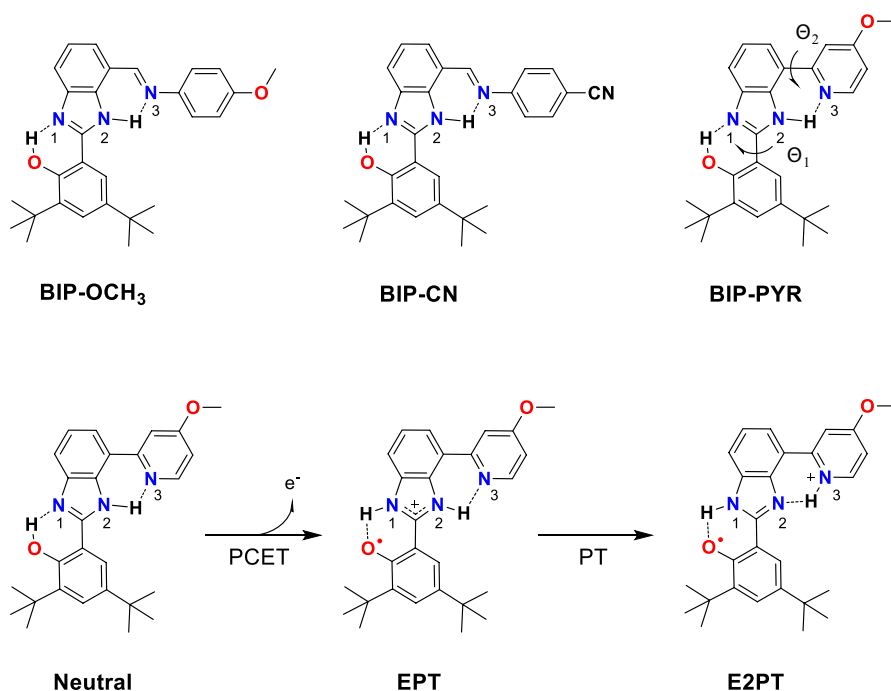


**Fig. 1** Top: molecular structures of the three studied benzimidazole-phenol (BIP) derivatives. The dihedral angles  $\Theta_1$  and  $\Theta_2$  are defined as shown for BIP-PYR. All depicted structures have angles  $\Theta_1$  and  $\Theta_2$  both at  $0^\circ$ . Bottom: electrochemical oxidation of the diamagnetic neutral BIP-PYR molecule yields one-proton transfer product (EPT; protonation state  $N_1N_2$ ) and two-proton transfer product (E2PT; protonation state  $N_1N_3$ ), both of which are paramagnetic (EPR-active) cation radicals. Analogous PCET and PT reactions occur for BIP-OCH<sub>3</sub> and BIP-CN

takes place in the vicinity of the phenoxyl oxygen atom (which carries the highest amount of unpaired spin), the second proton transfer follows at more remote sites (see Fig. 1). In this work, we use these unique systems to carry out computational studies to investigate the sensitivity of the magnetic resonance parameters to EPT and E2PT, as well as conformational substates of the model molecular complexes in aprotic environment.

## 2 Methods

Initial structures for BIP-OCH<sub>3</sub>, BIP-CN, and BIP-PYR (Fig. 1) were built and optimized in PQSMol using DFT with B3LYP//6-31G\* [56–58]. After initial optimization, structures were then re-optimized in Turbomole using B3LYP//def2-TZVPP with the D3BJ correction (Becke–Johnson damping) to account for dispersion effects [59–63]. Geometry optimizations were performed both for the neutral parent molecule (singlet, diamagnetic) as well as +1 cation radical (doublet, paramagnetic, EPR-active). Optimized N<sub>1</sub>N<sub>3</sub> (only N<sub>1</sub> and N<sub>3</sub> nitrogen atoms are protonated), N<sub>1</sub>N<sub>2</sub> (only N<sub>1</sub> and N<sub>2</sub> nitrogen atoms are protonated), ON<sub>2</sub> (phenol oxygen and N<sub>2</sub> nitrogen atom are protonated), and ON<sub>3</sub> (phenol oxygen and N<sub>3</sub> nitrogen atom are protonated) structures for all three compounds were then checked for the absence of imaginary frequencies at the same level of theory and found to be energetic minima. Magnetic resonance parameters (*g*-tensors and hyperfine coupling (HFC) tensors) were calculated with ORCA v. 4.2.1 [64, 65] using DFT B3LYP//EPRII. While the majority of calculations were performed in vacuum, the +1 cation BIP-CN in all protonation states was also optimized with the CPCM solvation model with dichloromethane parameters (ORCA keyword: CH2Cl2) and water parameters (ORCA keyword: water) [66]. These test calculations yielded magnetic resonance parameters and relative energy differences very similar to the vacuum results (see Sect. 3 below and Supporting Information Table S2). To investigate the effect of dihedral rotation on the EPR parameters, torsional scans of both  $\Theta_1$  and  $\Theta_2$  (see Fig. 1) were performed in Turbomole for multiple protonation states for the +1 cations using DFT with B3LYP//def2-TZVP with D3BJ dispersion correction fixing only the rotated dihedral angle and allowing all other coordinates to relax to obtain the torsional scan data.

## 3 Result and Discussion

The three BIP derivatives shown in Fig. 1 (BIP-OCH<sub>3</sub>, BIP-CN, and BIP-PYR) present models for Tyr–His pairs and thus provide the possibility to study both EPT (ON<sub>2</sub>→N<sub>1</sub>N<sub>2</sub>) and E2PT (ON<sub>2</sub>→N<sub>1</sub>N<sub>3</sub>). The structures are labeled with reference to where the two “mobile” protons are located (Fig. 1). Proton transfer/s occur after single oxidation of the neutral diamagnetic parent complex, yielding an EPR-active radical cation. In agreement with prior work [44, 52–54], the neutral parent molecule is stable in the ON<sub>2</sub> protonation state (see Supporting Information for energies). For the radical cation, calculated *g*-values, HFC tensors,

**Table 1** Calculated energies relative to the lowest energy structure and calculated EPR parameters for the +1 cations of BIP-OCH<sub>3</sub>, BIP-CN, and BIP-PYR (Fig. 1) in multiple protonation states

Molecule/protonation state	$\Delta E$ (kcal/mol)	<i>g</i> -Values	HFC <sup>14</sup> N <sub>1</sub> (MHz)	HFC <sup>14</sup> N <sub>2</sub> (MHz)	HFC <sup>14</sup> N <sub>3</sub> (MHz)
BIP-OCH <sub>3</sub>	N <sub>1</sub> N <sub>3</sub>	2.0023, 2.0044, 2.0073	-0.10, -0.32, +6.14	-0.40, -0.77, +2.54	-0.04, -0.10, +0.77
	N <sub>1</sub> N <sub>2</sub>	2.0023, 2.0043, 2.0072	-0.37, -0.72, +3.59	-0.08, +0.08, +5.22	-0.05, -0.10, +0.36
	ON <sub>2</sub>	2.0023, 2.0036, 2.0044	+0.19, -0.64, -0.86	-0.95, -1.04, +5.54	-0.06, +0.51, +6.18
BIP-CN	ON <sub>3</sub>	2.0023, 2.0038, 2.0043	-0.67, -0.77, +6.55	-1.22, -1.54, +4.37	-0.08, -0.18, +0.41
	N <sub>1</sub> N <sub>3</sub>	2.0023, 2.0044, 2.0072	-0.00, -0.23, +5.17	-0.16, -0.52, +3.14	-0.07, -0.12, +0.56
	N <sub>1</sub> N <sub>2</sub>	2.0023, 2.0043, 2.0071	-0.19, -0.53, +4.05	-0.03, +0.16, +4.59	-0.04, +0.04, -0.07
BIP-PYR	ON <sub>2</sub>	2.0023, 2.0037, 2.0043	-1.03, -1.40, +6.83	-0.03, +0.03, -1.17	-0.00, +0.01, -0.03
	ON <sub>3</sub>	2.0023, 2.0038, 2.0045	-0.45, -0.57, +5.15	-1.11, -1.48, +5.56	-0.08, -0.15, -0.16
	N <sub>1</sub> N <sub>3</sub>	2.0023, 2.0044, 2.0072	-0.04, -0.10, -0.15	-0.44, -0.81, +1.55	-0.08, -0.27, +5.44
BIP-PYR	N <sub>1</sub> N <sub>2</sub>	2.0023, 2.0043, 2.0071	-0.04, -0.09, -0.09	-0.41, -0.77, +2.71	+0.07, -0.08, +4.05
	ON <sub>2</sub>	2.0023, 2.0037, 2.0043	-0.01, -0.08, -0.41	-1.14, -1.52, +5.89	-0.87, -0.87, +0.97
	ON <sub>3</sub>	2.0023, 2.0038, 2.0044	-0.14, -0.23, -0.24	-1.29, -1.63, +3.17	-0.64, -0.72, +5.98

Structures were optimized using DFT with B3LYP-D3BJ/def2-TZVPP. EPR parameters were calculated using DFT with B3LYP/EPRII. Principal components of the hyperfine coupling (HFC) tensor are listed. Protonation states like N<sub>1</sub>N<sub>3</sub> indicate that both N<sub>1</sub> and N<sub>3</sub> are bonded to a hydrogen atom

and energies relative to the lowest energy state are shown in Table 1. Geometries and energies for BIP-CN and BIP-OCH<sub>3</sub> are in good agreement with previous computational studies [52, 54]. All three molecules in all investigated protonation states show only minimal deviations from planarity. For all three molecules, the N<sub>1</sub>N<sub>3</sub> protonation state has the lowest energy, the N<sub>1</sub>N<sub>2</sub> protonation state is a few kcal higher in energy, and protonation states with the phenoxy oxygen protonated (ON<sub>2</sub> and ON<sub>3</sub>) are much higher (> 9 kcal/mol) in energy. When BIP-OCH<sub>3</sub> is electrochemically oxidized, only the E2PT product (N<sub>1</sub>N<sub>3</sub>) can be detected, and when the BIP-CN is electrochemically oxidized, a mixture of EPT (N<sub>1</sub>N<sub>2</sub>) and E2PT (N<sub>1</sub>N<sub>3</sub>) products is generated, with the EPT being the majority product. This is in agreement with our DFT calculation where the N<sub>1</sub>N<sub>3</sub>–N<sub>1</sub>N<sub>2</sub> energy difference is 3.5 kcal/mol larger for BIP-OCH<sub>3</sub> than for BIP-CN. The energy difference between N<sub>1</sub>N<sub>3</sub> and N<sub>1</sub>N<sub>2</sub> protonation states for BIP-PYR is also only a few kcal/mol, but preliminary electrochemical studies have not demonstrated the presence of the EPT product. In any case, the energy difference calculated here between N<sub>1</sub>N<sub>3</sub> and N<sub>1</sub>N<sub>2</sub> protonation states lies within the accuracy range of DFT, which is several kcal/mol for this type of molecule [54, 67].

For all molecules, the orientation of principal *g*-tensor axes were as following: *g<sub>Z</sub>* is perpendicular to the plane of the molecule while *g<sub>Y</sub>* is parallel to a vector running between N<sub>3</sub> and carbon ortho to the phenoxy carbon and *g<sub>X</sub>* is approximately 45° rotated from the line connecting N<sub>1</sub> and N<sub>2</sub> (see Supporting Information, Figures S5 & S6). For the EPT product, the largest principal *g*-value *g<sub>X</sub>* is sensitive to the location of the proton since the *g*-values change substantially, around 0.003 from 2.004 to 2.007, as the proton is transferred from the oxygen to the nitrogen N<sub>1</sub> (the other mobile proton remains at N<sub>2</sub>). The middle *g*-value *g<sub>Y</sub>* is less sensitive, but shows the same trend, while the lowest *g*-value *g<sub>Z</sub>* is insensitive to the proton location and remains close to the free electron value. This is a well-known effect of the *g*-value dependence on the presence and strength of the O–H bond [68, 69]. The magnitude of changes in *g<sub>X</sub>* is easily experimentally detectable by HF EPR and has been recorded for a number of tyrosyl/phenoxy/nitroxide/semiquinone type systems [37, 38, 70–80].

On the other hand, the *g*-values are not influenced by the position of the second proton with respect to N<sub>2</sub> or N<sub>3</sub>. Due to the limited accuracy under typical conditions (*g*-strain, different glass conditions, and other broadening mechanisms) of experimental EPR data and the DFT calculations, the structures N<sub>1</sub>N<sub>2</sub> and N<sub>1</sub>N<sub>3</sub> are not distinguishable based on the *g*-value differences, which differ by only 0.0001. Thus, even EPR spectroscopy at very high frequencies cannot directly discriminate if the system has undergone the EPT or E2PT process. The spin density plots (Fig. 2) also do not show apparent differences between N<sub>1</sub>N<sub>2</sub> and N<sub>1</sub>N<sub>3</sub>, which means that <sup>14</sup>N hyperfine values are too similar to allow distinction of the two protonation states (Table 1). For N<sub>1</sub>N<sub>3</sub> and N<sub>1</sub>N<sub>2</sub>, the spin density is primarily located on the phenoxy group. In contrast, if the oxygen is protonated as for ON<sub>2</sub> and ON<sub>3</sub> configurations, the spin density is more delocalized extending to the benzimidazole group of BIP-PYR (Fig. 2). Comparable results were obtained for the two other complexes (see Supporting Information, Figures S1 and S2). In fact, in not a single case does the spin density extend past the benzimidazole group onto the imine or pyridine moiety

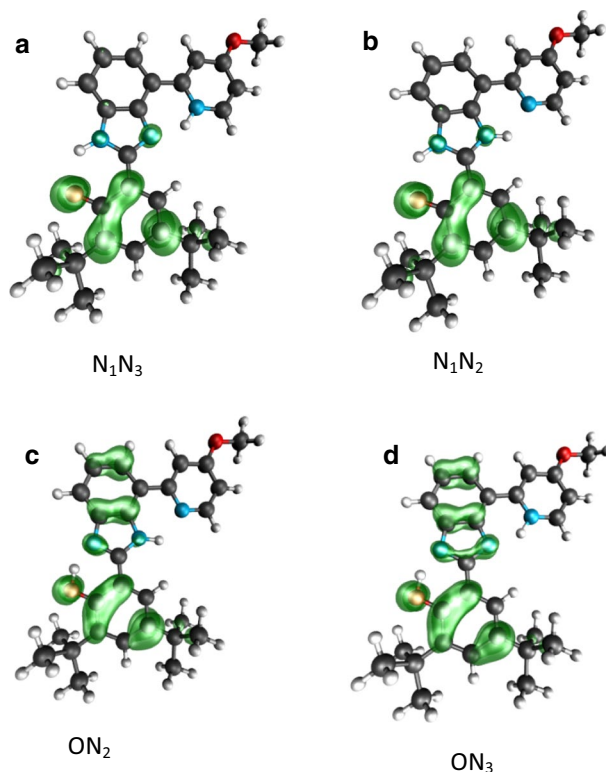


**Fig. 2** Optimized structures and spin densities at an isosurface of  $0.002 e/a_0^3$  for +1 cations of the BIP-PYR structure. Structures were optimized using DFT (B3LYP||def2-TZVPP with D3BJ). Four possible hydrogen positions are shown: **a**  $N_1N_3$ , **b**  $N_1N_2$ , **c**  $ON_2$ , and **d**  $ON_3$

indicating that further substitution of these groups, while it might change redox potentials, is unlikely to influence the magnetic resonance parameters of these complexes to any significant degree.

As a group, these constructs represent a versatile model system to understand complex proton transfer processes found in biological systems [44]. In proteins and model systems containing a redox-active Tyr residue, a significant spread of  $g_X$ -values was experimentally observed, while the  $g_Y$  and  $g_Z$ -values were essentially unchanged [68, 69]. Experimentally detected Tyr cation radical  $g_X$ -values vary between 2.009 to 2.006 [69]. The upper range is higher than the calculated  $g_X$ -values in the current work. Taking into account that structures like  $ON_2$  and  $ON_3$  are not stable for the oxidized Tyr and have not been observed experimentally, this extreme variation cannot be explained on the basis of different protonation states of remote nitrogen atoms (see Table 1). Furthermore, the spread is too large to be attributed only to the strength of the hydrogen bonds to the oxygen of Tyr, which is less than 0.002 for the extreme variation of the H-bond distance [68]. However, nature is typically very efficient in modifying the electronic properties of a protein-cofactor



system to fulfill the required specific catalytic needs often by forcing cofactor molecules or residues into conformations significantly different from what are observed in isotropic solutions. This raises the question whether this applies to the current examples: could the conformational state rather than the protonation state modulate magnetic resonance parameters of the radical complexes? To answer this question, we undertook additional conformational studies.

Rotation around several single bonds is possible for these complexes and leads to their conformation change, as shown in Fig. 1. The rotation around  $\Theta_2$ , with  $\Theta_1$  fixed in its energy minimized value near  $0^\circ$ , has a barrier ranging from 13 to 35 kcal/mol (Fig. 3, S3 and S4), and exhibits two low local minima differing by 8.5–11.7 kcal/mol. As shown in those figures, the  $g_X$ -values remain nearly constant and change by less than 0.0001 for all three systems, despite the substantial change in energy. This is not surprising since the imine moiety does not contain significant spin density (Fig. 2). In contrast, rotation around  $\Theta_1$  with  $\Theta_2$  remaining in its lowest energy conformation near  $0^\circ$  is shown in Fig. 4 for the BIP-PYR molecule. This rotation of the phenol group results in large increases in the  $g_X$ -values, by more than 0.001. The maximum energy changes for this rotation are on the order of 10 kcal/mol, although the actual differences in energies between the  $\Theta_1=0^\circ$  and  $\Theta_1=180^\circ$  conformations are approximately 6–8 kcal/mol. Similar changes in both energies and  $g_X$ -values are present for all three molecules (see Supporting Information). It can clearly be seen that when the oxygen atom is unable to form a hydrogen bond (note the  $\Theta_1=180^\circ$  structure for  $N_1N_3$  and the middle structure in  $N_1N_2$  where  $\Theta_1=80^\circ$ ), the  $g_X$  value increases by a measurable amount, ca. 0.0012. The rotational profile of  $\Theta_1$  for  $N_1N_2$

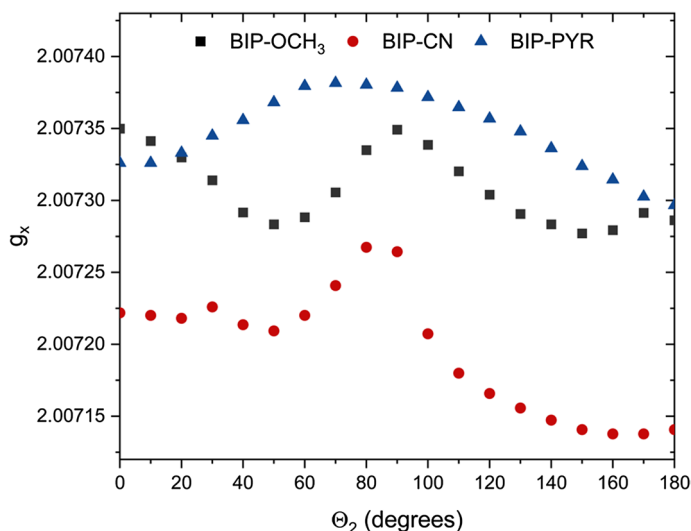


**Fig. 3** Effect of rotation around  $\Theta_2$  on  $g_X$ -values for three molecules in the  $N_1N_3$  structure with  $\Theta_1=0$  (the lowest energy structure). EPR  $g_X$ -values (B3LYP/IEPRII) were calculated from the constrained optimizations (B3LYP/def2-TZVP) with all degrees of freedom except the constrained dihedral allowed to relax

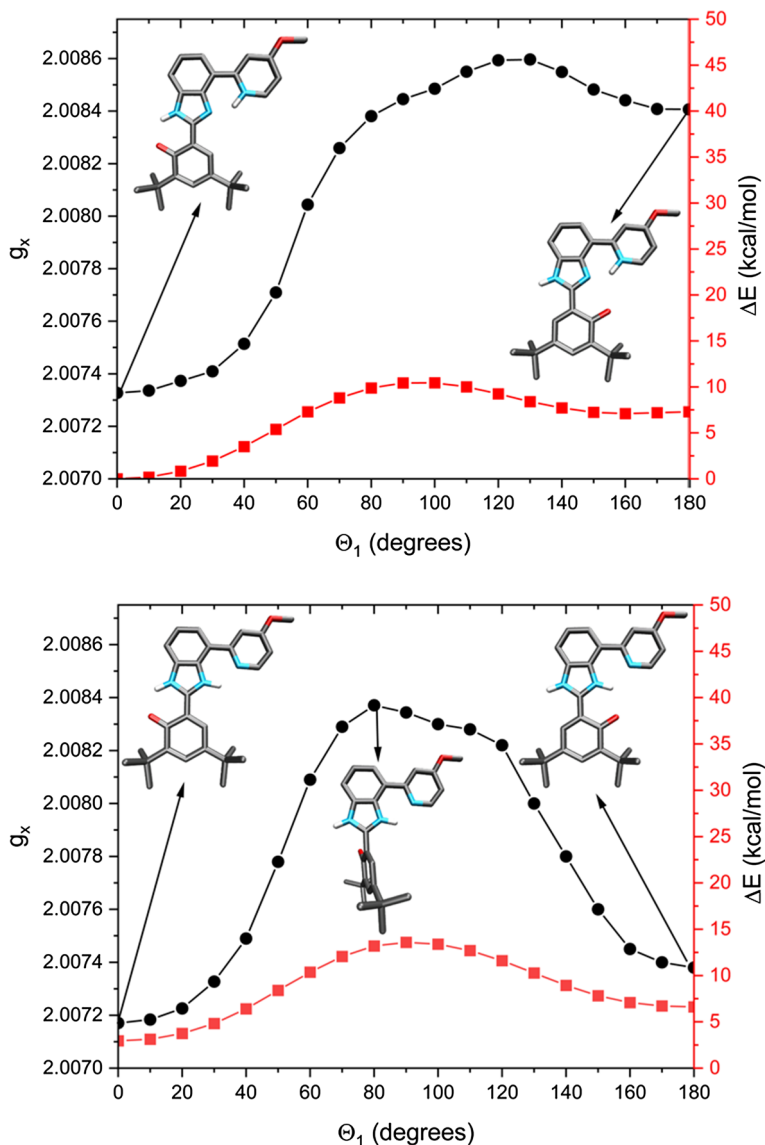


**Fig. 4** Effect of rotation around  $\Theta_1$  angle on the energy and the  $g_x$ -value for  $N_1N_3$  (top) and  $N_1N_2$  (bottom) for BIP-PYR. The energies are measured relative to the lowest energy  $N_1N_3$  conformation. The inset structures show conformations that correspond to the given  $g$ -values and energies

is, as expected, more symmetric than  $N_1N_3$ , since a  $180^\circ$  rotation for  $N_1N_2$  restores an H-bond to the phenoxyl oxygen.

Note that all calculations discussed above were done in vacuum, and thus imitate an aprotic environment, i.e., lack of external protons to make intermolecular H-bonds. For BIP-CN, we have explored the effect of changing solvent polarity,

without adding explicit hydrogen bonds, through implicit solvent models. Calculations were performed with CPCM, an implicit solvent model, mimicking intermediate polarity ( $\text{CH}_2\text{Cl}_2$ ) and a very polar environment ( $\text{H}_2\text{O}$ ). The relative energy differences were very similar to the vacuum results (Table S2). The changes in  $g$ -values were minor, at maximum deviating 0.0002 from the values obtained for calculations in vacuum. This demonstrates that explicit hydrogen bonds are needed to significantly alter magnetic resonance parameters and that absent conformational changes resulting in new or different hydrogen bonds, even large changes in polarity have only minor effects on those parameters.

Altogether, these calculations combined allow us to distinguish between changes to the  $g$ -values due to conformational effects and changes caused by additional hydrogen bonding to the oxygen. Analysis of the data reveals that the calculated changes in the  $g_X$ -values for different conformation states are directly related to the distance of the spin density carrying oxygen from the proton on the  $\text{N}_1$  and  $\text{N}_2$  positions. If the conformation itself is additionally contributing to the modulation of the  $g_X$ , this effect is minor and cannot be decisively confirmed due to the current accuracy of the experimental and theoretical approaches. Thus, the presence of lower  $g$ -values in many proteins cannot simply be explained with the rotation of the phenoxyl group. The best candidate for lowering  $g_X$  is the introduction of additional, weaker H-bonds from proton donating molecules, which was not addressed in the current calculations. One of the best studied protein cofactors in the protic environment are quinones. It was shown in prior work [70, 72–74, 81, 82] that the addition of extra H-bonds can lead to a substantial lowering of  $g_X$ .

To summarize, in this work we presented theoretical calculations to investigate the sensitivity of the magnetic resonance parameters to the one-electron one-proton and one-electron multiple proton transfers, as well as conformational substates of a model molecular complex in an aprotic environment. As model compounds, we used recently developed systems which mimic PCET in biologically relevant Tyr–His couples [44, 52–54]. Upon oxidation of the phenol, which operates as the Tyr analog (Scheme 1), these complexes can perform not only one-electron one-proton transfer, EPT, but also one-electron two-proton transfer, E2PT (Fig. 1). While the first proton transfer takes place in the vicinity of the phenoxyl oxygen, a second proton transfer occurs at a more remote site. It was shown that while  $g_X$  components of the  $g$ -tensors are very sensitive to EPT, which leads to the change of  $g_X$ -value up to 0.003, it is not sensitive to the second proton transfer. In the last case, the change of the  $g_X$ -value is only ca. 0.0001, which is too small to be definitely assigned by HF EPR taking into account the typical accuracy of the experiment, broad EPR line width of the tyrosyl type radical, and the accuracy of the DFT calculations. As for  $^{14}\text{N}$  hyperfine couplings, they are also too similar to allow distinction of the EPT from E2PT configuration. We also tested the hypothesis that conformational changes of the model complexes can lead to the modulation of the  $g$ -values. For this reason, we calculated magnetic resonance parameters as a function of the rotation angles around single bonds,  $\Theta_1$  and  $\Theta_2$  (Fig. 1). It was demonstrated that while rotation around  $\Theta_2$  has only a negligible effect on  $g$ -values, less than 0.0001, rotation of the phenol group around  $\Theta_1$  results in large positive changes in the  $g_X$ -values, by more than 0.001. Analysis of the data reveals that the main source of these changes is

related to the strength of the H-bond between the phenoxyl oxygen and the proton in the N<sub>1</sub> and N<sub>2</sub> positions. Calculations with solvent environment of different polarity showed that explicit hydrogen bonds are needed to significantly alter magnetic resonance parameters and even large changes in polarity have only minor effects on those parameters.

These findings decrease the likelihood of misinterpretation of the high-frequency EPR data of electron transfer in the Tyr-containing systems and permit more robust mechanistic studies in biological as well as bio-inspired model systems.

**Acknowledgements** This study is based upon work supported by U.S. Department of Energy, Office of Science, Office of Basic Energy Sciences, Division of Chemical Sciences, Geosciences, and Biosciences, under contract number DE-AC02-06CH11357 at Argonne National Laboratory (JN and OGP) and DE-FG02-03ER15393 (ALM and TAM). The work was supported by the Illinois Space Grant Consortium and National Institutes of Health (SC3 GM122614) (HO and KLM). We gratefully acknowledge the computing resources provided on Blues and Bebop, high-performance computing clusters operated by the Laboratory Computing Resource Center at Argonne National Laboratory.

## References


1. K.-P. Dinse, G. Jeschke, *Methods in Physical Chemistry* (Wiley-VCH Verlag GmbH & Co. KGaA, Weinheim, 2012), pp. 159–189
2. D. Goldfarb, S. Stoll (eds.), *EPR Spectroscopy: Fundamentals and Methods* (Wiley, New York, 2018)
3. S.K. Misra (ed.), *Multifrequency Electron Paramagnetic Resonance: Theory and Applications* (Wiley-VCH Verlag GmbH & Co. KGaA, Weinheim, 2011)
4. K. Möbius, A. Savitsky, *High-Field EPR Spectroscopy on Proteins and Their Model Systems: Characterization of Transient Paramagnetic States* (The Royal Society of Chemistry, Cambridge, 2009)
5. A. Lund, M. Shiotani, S. Shimada, *Principles and Applications of ESR Spectroscopy* (Springer, Dordrecht, 2011)
6. A. Schweiger, G. Jeschke, *Principles of Pulse Electron Paramagnetic Resonance* (Oxford University Press, New York, 2001)
7. J.A. Weil, J.R. Bolton, J.A. Weil, J.R. Bolton, J.E. Wertz, *Electron Paramagnetic Resonance: Elementary Theory and Practical Applications* (Wiley, New York, 2007)
8. M. Drescher, G. Jeschke (eds.), *EPR Spectroscopy: Applications in Chemistry and Biology* (Springer, Berlin, 2012)
9. G.R. Eaton, S.S. Eaton, K.M. Salikhov (eds.), *Foundations of Modern EPR* (World Scientific Publishing, Singapore, 1998)
10. J. Niklas, O.G. Poluektov, *Adv. Energy Mater.* **7**, 1602226 (2017)
11. K. Möbius, W. Lubitz, N. Cox, A. Savitsky, *Magnetochemistry* **4**, 85 (2018)
12. F. Gerson, W. Huber, *Electron Spin Resonance Spectroscopy of Organic Radicals* (Wiley-VCH, Weinheim, 2003)
13. H. Kurreck, B. Kirste, W. Lubitz, *Angew. Chem. Int. Edit.* **23**, 173–194 (1984)
14. H. Kurreck, B. Kirste, W. Lubitz, *Electron Nuclear Double Resonance Spectroscopy of Radicals in Solution—Applications to Organic and Biological Chemistry* (VCH Publishers Inc., Deerfield Beach, 1988)
15. K. Möbius, W. Fröhling, F. Lenzian, W. Lubitz, M. Plato, C.J. Winscom, *J. Phys. Chem.* **86**, 4491–4507 (1982)
16. G. Jeschke, *ChemPhysChem* **3**, 927–932 (2002)
17. C. Gemperle, A. Schweiger, *Chem. Rev.* **91**, 1481–1505 (1991)
18. A. Savitsky, K. Möbius, *Photosynth. Res.* **102**, 311–333 (2009)
19. O. Grinberg, L.J. Berliner (eds.), *Very High Frequency (VHF) ESR/EPR*, vol. 22 (Springer, New York, 2004)
20. L. Kulik, W. Lubitz, *Photosynth. Res.* **102**, 391–401 (2009)

21. Y.S. Lebedev, *Appl. Magn. Reson.* **7**, 339–362 (1994)
22. O.Y. Grinberg, A.A. Dubinskii, in *Very High Frequency (VHF) ESR/EPR*, vol. 22, ed. by O. Grinberg, L.J. Berliner (Springer, New York, 2004), pp. 1–18
23. A.A. Galkin, O.Y. Grinberg, A.A. Dubinskii, N.N. Kabdin, V.N. Krymov, V.I. Kurochkin, Y.S. Lebedev, L.F. Oranskii, V.F. Shuvalov, *Instrum. Exp. Tech.* **20**, 1229–1229 (1977)
24. A.Y. Bresgunov, A.A. Dubinskii, V.N. Krimov, Y.G. Petrov, O.G. Poluektov, Y.S. Lebedev, *Appl. Magn. Reson.* **2**, 715–728 (1991)
25. O.Y. Grinberg, A.A. Dubinskii, Y.S. Lebedev, *Usp. Khim.* **52**, 1490–1513 (1983)
26. C. Rudowicz, S.K. Misra, *Appl. Spectrosc. Rev.* **36**, 11–63 (2001)
27. F. Neese, *Multifrequency Electron Paramagnetic Resonance* (Wiley-VCH Verlag GmbH & Co. KGaA, Weinheim, 2011), pp. 295–326
28. M. Kaupp, M. Bühl, V.G. Malkin (eds.), *Calculation of NMR and EPR Parameters: Theory and Applications* (Wiley-VCH, Weinheim, 2004)
29. F. Neese, in *High Resolution EPR: Applications to Metalloenzymes and Metals in Medicine*, ed. by L. Berliner, G. Hanson (Springer New York, New York, 2009), pp. 175–229
30. F. Neese, *Coord. Chem. Rev.* **253**, 526–563 (2009)
31. M.L. Munzarova, P. Kubacek, M. Kaupp, *J. Am. Chem. Soc.* **122**, 11900–11913 (2000)
32. M. Munzarova, M. Kaupp, *J. Phys. Chem. A* **103**, 9966–9983 (1999)
33. M. Retegan, N. Cox, W. Lubitz, F. Neese, D.A. Pantazis, *Phys. Chem. Chem. Phys.* **16**, 11901–11910 (2014)
34. G.T. Babcock, M. Espe, C. Hoganson, N. LydakisSimantiris, J. McCracken, W.J. Shi, S. Styring, C. Tommos, K. Warncke, *Acta Chem. Scand.* **51**, 533–540 (1997)
35. D.L. Jenson, B.A. Barry, *J. Am. Chem. Soc.* **131**, 10567–10573 (2009)
36. B.A. Barry, *Biochim. Biophys. Acta Bioenerg.* **1847**, 46–54 (2015)
37. S. Un, P. Dorlet, A.W. Rutherford, *Appl. Magn. Reson.* **21**, 341–361 (2001)
38. P. Faller, C. Goussias, A.W. Rutherford, S. Un, *Proc. Natl. Acad. Sci. USA* **100**, 8732–8735 (2003)
39. R.E. Blankenship, *Molecular Mechanisms of Photosynthesis* (Blackwell Science Limited, Oxford, 2002)
40. T.J. Wydrzynski, K. Satoh (eds.), *Photosystem II—The Light-Driven Water: Plastoquinone Oxidoreductase*, vol. 22 (Springer, Dordrecht, 2005)
41. Y. Umena, K. Kawakami, J.R. Shen, N. Kamiya, *Nature* **473**, 55–60 (2011)
42. P. Faller, R.J. Debus, K. Brettel, M. Sugiura, A.W. Rutherford, A. Boussac, *Proc. Natl. Acad. Sci. USA* **98**, 14368–14373 (2001)
43. R. Chatterjee, C.S. Coates, S. Milikisiyants, C.I. Lee, A. Wagner, O.G. Poluektov, K.V. Lakshmi, *Biochemistry* **52**, 4781–4790 (2013)
44. S.J. Mora, E. Odella, G.F. Moore, D. Gust, T.A. Moore, A.L. Moore, *Acc. Chem. Res.* **51**, 445–453 (2018)
45. J.D. Megiatto, D.D. Mendez-Hernandez, M.E. Tejada-Ferrari, A.L. Teillout, M.J. Llansola-Portoles, G. Kodis, O.G. Poluektov, T. Rajh, V. Mujica, T.L. Groy, D. Gust, T.A. Moore, A.L. Moore, *Nat. Chem.* **6**, 423–428 (2014)
46. D.A. Svistunenko, *Biochim. Biophys. Acta Bioenerg.* **1707**, 127–155 (2005)
47. A. Migliore, N.F. Polizzi, M.J. Therien, D.N. Beratan, *Chem. Rev.* **114**, 3381–3465 (2014)
48. J. Stubbe, W.A. van der Donk, *Chem. Rev.* **98**, 705–762 (1998)
49. L. Hammarström, S. Styring, *Energy Environ. Sci.* **4**, 2379–2388 (2011)
50. H.B. Gray, J.R. Winkler, *Acc. Chem. Res.* **51**, 1850–1857 (2018)
51. S.Y. Reece, D.G. Nocera, *Annu. Rev. Biochem.* **78**, 673–699 (2009)
52. E. Odella, S.J. Mora, B.L. Wadsworth, J.J. Goings, M.A. Gervaldo, L.E. Sereno, T.L. Groy, D. Gust, T.A. Moore, G.F. Moore, S. Hammes-Schiffer, A.L. Moore, *Chem. Sci.* **11**, 3820–3828 (2020)
53. E. Odella, B.L. Wadsworth, S.J. Mora, J.J. Goings, M.T. Huynh, D. Gust, T.A. Moore, G.F. Moore, S. Hammes-Schiffer, A.L. Moore, *J. Am. Chem. Soc.* **141**, 14057–14061 (2019)
54. E. Odella, S.J. Mora, B.L. Wadsworth, M.T. Huynh, J.J. Goings, P.A. Liddell, T.L. Groy, M. Gervaldo, L.E. Sereno, D. Gust, T.A. Moore, G.F. Moore, S. Hammes-Schiffer, A.L. Moore, *J. Am. Chem. Soc.* **140**, 15450–15460 (2018)
55. M.T. Huynh, S.J. Mora, M. Villalba, M.E. Tejada-Ferrari, P.A. Liddell, B.R. Cherry, A.L. Teillout, C.W. Machan, C.P. Kubiak, D. Gust, T.A. Moore, S. Hammes-Schiffer, A.L. Moore, *ACS Cent. Sci.* **3**, 372–380 (2017)
56. P.J. Stephens, F.J. Devlin, C.F. Chabalowski, M.J. Frisch, *J. Phys. Chem.* **98**, 11623–11627 (1994)
57. A.D. Becke, *J. Chem. Phys.* **98**, 5648–5652 (1993)

58. J. Baker, T. Janowski, K. Wolinski, P. Pulay, *Wiley Interdiscip. Rev. Comput. Mol. Sci.* **2**, 63–72 (2012)
59. S.G. Balasubramani, G.P. Chen, S. Coriani, M. Diedenhofen, M.S. Frank, Y.J. Franzke, F. Furche, R. Grotjahn, M.E. Harding, C. Hattig, A. Hellweg, B. Helmich-Paris, C. Holzer, U. Huniar, M. Kaupp, A.M. Khah, S.K. Khani, T. Müller, F. Mack, B.D. Nguyen, S.M. Parker, E. Perlt, D. Rappoport, K. Reiter, S. Roy, M. Rückert, G. Schmitz, M. Sierka, E. Tapavicza, D.P. Tew, C. Wüllen, V.K. Voora, F. Weigend, A. Wodyński, J.M. Yu, *J. Chem. Phys.* **152**, 36 (2020)
60. F. Weigend, R. Ahlrichs, *Phys. Chem. Chem. Phys.* **7**, 3297–3305 (2005)
61. F. Furche, R. Ahlrichs, C. Hattig, W. Klopper, M. Sierka, F. Weigend, *Wiley Interdiscip. Rev. Comput. Mol. Sci.* **4**, 91–100 (2014)
62. S. Grimme, S. Ehrlich, L. Goerigk, *J. Comput. Chem.* **32**, 1456–1465 (2011)
63. S. Grimme, J. Antony, S. Ehrlich, H. Krieg, *J. Chem. Phys.* **132**, 154104 (2010)
64. F. Neese, *Wiley Interdiscip. Rev. Comput. Mol. Sci.* **8**, 6 (2018)
65. F. Neese, *Wiley Interdiscip. Rev. Comput. Mol. Sci.* **2**, 73–78 (2012)
66. V. Barone, M. Cossi, *J. Phys. Chem. A* **102**, 1995–2001 (1998)
67. M. Steinmetz, A. Hansen, S. Ehrlich, T. Risthaus, S. Grimme, in *Density Functionals: Thermochemistry*, ed. by E.R. Johnson (Springer International Publishing, Cham, 2015), pp. 1–23
68. D. Svistunenko, M. Adelus, M. Dawson, P. Robinson, C. Bernini, A. Sinicropi, R. Basosi, *Stud. Univ. Babeş Bolyai Chem.* **56**, 135–146 (2011)
69. D.A. Svistunenko, C.E. Cooper, *Biophys. J.* **87**, 582–595 (2004)
70. S. Sinnecker, E. Reijerse, F. Neese, W. Lubitz, *J. Am. Chem. Soc.* **126**, 3280–3290 (2004)
71. G.J. Gerfen, B.F. Bellew, S. Un, J.M. Bollinger, J. Stubbe, R.G. Griffin, D.J. Singel, *J. Am. Chem. Soc.* **115**, 6420–6421 (1993)
72. J.R. Asher, M. Kaupp, *Theor. Chem. Acc.* **119**, 477–487 (2008)
73. J.R. Asher, N.L. Doltsinis, M. Kaupp, *Magn. Reson. Chem.* **43**, S237–S247 (2005)
74. J.R. Asher, N.L. Doltsinis, M. Kaupp, *J. Am. Chem. Soc.* **126**, 9854–9861 (2004)
75. S. Un, M. Atta, M. Fontecave, A.W. Rutherford, *J. Am. Chem. Soc.* **117**, 10713–10719 (1995)
76. L. Benisvy, R. Bittl, E. Bothe, C.D. Garner, J. McMaster, S. Ross, C. Teutloff, F. Neese, *Angew. Chem. Int. Edit.* **44**, 5314–5317 (2005)
77. T.I. Smirnova, A.I. Smirnov, S.V. Paschenko, O.G. Poluektov, *J. Am. Chem. Soc.* **129**, 3476–3477 (2007)
78. T.I. Smirnova, T.G. Chadwick, M.A. Voinov, O. Poluektov, J. van Tol, A. Ozarowski, G. Schaaf, M.M. Ryan, V.A. Bankaitis, *Biophys. J.* **92**, 3686–3695 (2007)
79. K. Möbius, A. Savitsky, C. Wegener, M. Plato, M. Fuchs, A. Schnegg, A.A. Dubinskii, Y.A. Grishin, I.A. Grigor'ev, M. Kuhn, D. Duché, H. Zimmermann, H.J. Steinhoff, *Magn. Reson. Chem.* **43**, S4–S19 (2005)
80. M. Plato, H.J. Steinhoff, C. Wegener, J.T. Topping, A. Savitsky, K. Möbius, *Mol. Phys.* **100**, 3711–3721 (2002)
81. S. Sinnecker, A. Rajendran, A. Klamt, M. Diedenhofen, F. Neese, *J. Phys. Chem. A* **110**, 2235–2245 (2006)
82. M. Witwicki, J. Jezierska, A. Ozarowski, *Chem. Phys. Lett.* **473**, 160–166 (2009)

**Publisher's Note** Springer Nature remains neutral with regard to jurisdictional claims in published maps and institutional affiliations.

## Affiliations

Kristy L. Mardis<sup>2</sup> · Jens Niklas<sup>1</sup>  · Harriet Omodayo<sup>2</sup> · Emmanuel Odella<sup>3</sup> · Thomas A. Moore<sup>3</sup> · Ana L. Moore<sup>3</sup> · Oleg G. Poluektov<sup>1</sup> 

✉ Oleg G. Poluektov  
Oleg@anl.gov

<sup>1</sup> Chemical Sciences and Engineering Division, Argonne National Laboratory, Lemont, IL 60439, USA

- 
- <sup>2</sup> Department of Chemistry, Physics, and Engineering Studies, Chicago State University, Chicago, IL 60628, USA
- <sup>3</sup> School of Molecular Sciences, Arizona State University, Tempe, AZ 85287, USA